Available online at www.sciencedirect.com
SCIENCE DIRECT®
Journal of the European Ceramic Society 25 (2005) 3323–3334
www.elsevier.com/locate/jeurceramsoc

PZT prepared by spray drying: From powder synthesis to electromechanical properties

F. Bezzi[a,b,1], A.L. Costa[a,b,*], D. Piazza[a,b], A. Ruffini[a,b], S. Albonetti[a,b], C. Galassi[a,b]

[a] *CNR-ISTEC, Institute of Science and Technology for Ceramics, National Research Council, I-48018 Faenza, Italy*
[b] *Faculty of Industrial Chemistry, University of Bologna, I-40126 Bologna, Italy*

Received 22 February 2004; received in revised form 2 August 2004; accepted 15 August 2004
Available online 19 November 2004

Abstract

A PZT niobium-doped material (PZTN) was developed from precursor powders obtained by spray drying of water solution of Zr and Pb nitrates, Ti isopropoxide and Nb–ammonium complex. The thermo-oxidative process as well as the phase evolution were analysed. The morphology of powders was investigated as a function of the spray-drying conditions. The stoichiometry of the systems was checked at each stage of the process and no fluctuation was detected. The obtained powders had a spherical, hollow and porous structure and were transformed into a pure perovskite phase at 550 °C. The samples, sintered at 1100 °C for 2 h in air showed 98% relative density at densification temperature of 100 °C lower than following the conventional mixed oxide route. The green and final densities were improved by introducing a grinding step and high pressure cold isostatic consolidation. Some sintered samples were fully densified by hot isostatic pressing (1100 °C, 300 bars) post-treatment, obtaining pore free structures. The electrical characterisation showed comparable or better properties than those obtained with the mixed oxide method.

Keywords: Spray drying; Chemical route; PZT; Precursor solution; Densification; Electrical properties

1. Introduction

Non-conventional processing of PZT bulk materials attracts attention for the relevant technological benefits of reducing the reaction and sintering temperature and improving chemical homogeneity. Several chemical routes have been investigated to enhance homogeneity, purity and microstructure of the material and to better control the stoichiometry. Among these, methods based on precipitation–filtration, such as coprecipitation[1–4] and hydrothermal[5–8] or sol–gel[9–12] synthesis, were extensively applied even if they can induce the segregation of the components during the precipitation or gelation process. The segregation can be limited at the droplet level and chemically homogenous powders can be obtained by breaking the solution into small droplets. These methods include solution aerosol processes, freeze–drying and emulsion drying, the only requirement being the availability of stable solutions of the starting cations. In particular the chemical synthesis of niobium-doped compositions is limited by the difficulty of finding commercially available niobium soluble salts.[13] Methods like spray pyrolisis[14–16] or two-stages thermal processes by spray-drying[17–20] are worthy of further investigation.

The solution spray drying is a solvent vaporisation method very promising for the synthesis of multi-component systems based on metal oxides.[21,22] The solution is atomised into small droplets and injected into the hot chamber of the dryer. The powder is then thermally treated until the desired phase is formed. Furthermore the spray-drying is a widely applied

* Corresponding author.
E-mail address: annacosta@istec.cnr.it (A.L. Costa).
[1] Now at ENEA, Centro di Ricerche Nuovi Materiali (Faenza), Italy.

0955-2219/$ – see front matter © 2004 Elsevier Ltd. All rights reserved.
doi:10.1016/j.jeurceramsoc.2004.08.027

technique in the ceramic industry and so suitable of industrial application.

The possible morphologies of particles derived by solution aerosol techniques have been reviewed by Messing et al.[23] Typically, the powders consist of hollow, shell-like aggregates of submicrometric primary particles due to the surface precipitation as a consequence of the solute concentration gradient during the condensation step.[24]

In this study PZT niobium-doped powder was synthesised by spray drying of the precursor solution, followed by thermal treatment and characterisation. The stoichiometry was carefully controlled at the different stages of the preparation and the morphology of the spray-dried agglomerates was correlated to that of the as-sprayed raw materials. The densification was optimised and microstructure and piezoelectric properties were investigated. They are discussed in comparison with the properties of the same material produced by the conventional "mixed oxides" procedure. Hot isostatic pressing of as-sintered samples was also performed in order to eliminate the residual voids that can be a consequence of the morphology of the as-sprayed powders.

2. Experimental procedure

2.1. Precursor solutions (PS)

Aqueous solutions of Nb–ammonium complex (AD/1440: Nb_2O_5 25.6%, CBMM-Companhia Brasileira de Metalurgia e Mineração), $ZrO(NO_3)_2{\cdot}nH_2O$ (99%, Aldrich), $Pb(NO_3)_2$ (99%, Fluka) and $Ti[OCH(CH_3)_2]_4$ (97%, Aldrich) were prepared separately in order to study the stability over time and the morphology of the precursors separately sprayed. The niobium precursor was dissolved (≅0.04 M) in a nitric acid solution (Carlo Erba Reagenti, 65 wt.%, ≅0.4 M) adding hydrogen peroxide (Polichimica, 35 wt.%, ≅0.3 M). The addition of hydrogen peroxide promotes the solubility of hydrated niobia forming more soluble yellow peroxo-niobium complexes.[25] Zirconium (≅0.1 M) and lead (≅0.2 M) nitrate solutions were prepared by dissolution of the respective salts in nitric acid solution (≅0.1 M). The acid environment insures the solubility of hydrated cations as reported in literature.[26] The titanium solution (≅0.15 M) was prepared by dissolution of $Ti[OCH(CH_3)_2]_4$ (97%) in nitric acid (≅2 M) and H_2O_2 (≅0.35 M). The precursor solution of the chosen PZTN composition was obtained by adding dropwise the solution of titanium to the niobium solution until hydrated titania solubilised. Then the zirconium and lead nitrate solutions were added to the mixture following the expected stoichiometric ratios.

2.2. Powder synthesis, calcination and densification

Powders of the composition $Pb_{0.988}[(Zr_{0.52}, Ti_{0.48})_{0.976}Nb_{0.024}]O_3$ (PZTN) were prepared by spray drying the precursor solution (PS) followed by calcination (SD method). The as prepared PS, kept under stirring, was sprayed and dried in the laboratory spray drier (Mod. SD-05, Lab-Plant Ltd., Huddersfield, England) and the spray-drying parameters were optimised taking into account morphology of the powders and yield of the process. Two batches of powder were produced in the same conditions, the first resulting in a slight defect of titanium in comparison to stoichiometric composition, in the following indicated as 1, and the second with the exact composition within the calculated absolute error, indicated as 2. The processing conditions are schematically summarised in Fig. 1.

For the mixed oxide method (MO), the homogeneous chemical grade oxide mixture (PbO, ZrO_2, TiO_2 and Nb_2O_5) was calcined in air at 850 °C for 4 h and wet ball milled for 100 h with zirconia milling media.[27] The cold pressing performance of all the powders was improved by wetting with a dilute PEG 400 (Merck) solution followed by granulation. The powders were uniaxially (75 MPa) and isostatically (150 and 400 MPa for MO and SD powders, respectively) pressed

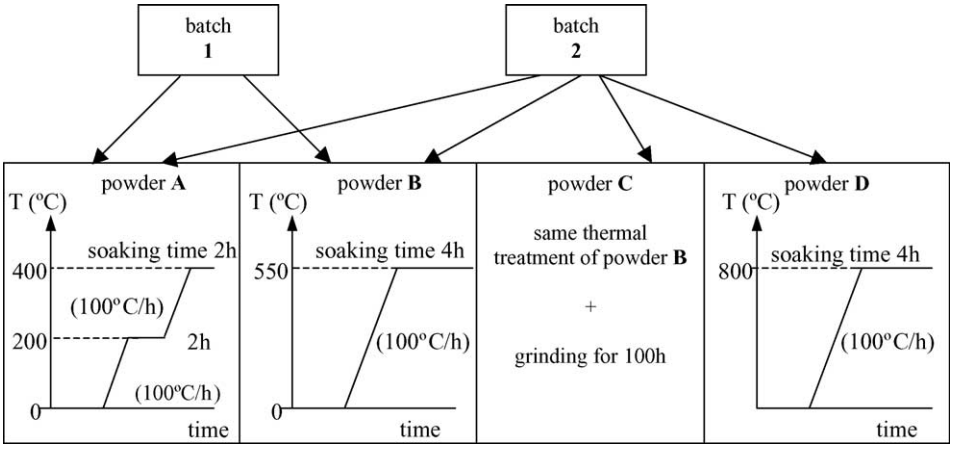

Fig. 1. Thermal treatments and processing conditions.

in disks (height 4 mm and diameter 14 mm). The samples were then sintered at 900–1100 °C (1200 °C for MO samples) for 2 h. In order to avoid the loss of PbO, that is very fast at temperatures over 1000 °C, all the sintering processes were done in a $PbZrO_3$ pack. To increase the density the pre-sintered sample was hot isostatically pressed at 1100 °C for 2 h at 30 MPa (HIP apparatus QIH 15, FPS, Sweden, Ar working gas).

2.3. Characterisation

The chemical composition of the solutions and of the as-sprayed and calcined powders was determined by inductively coupled plasma-atomic emission spectrometry (ICP-AES) (Liberty 200, Varian, Clayton South, Australia). The powder sample was dissolved by microwave-assisted acid treatment.[28] The thermogravimetry (TGA) and differential thermal analyses (DTA) were carried out on the as-sprayed PZTN powder at 10 °C/min heating rate with simultaneous thermal analyser (STA 409, Netzsch, Selb/Bavaria, Germany).

Powder morphology and microstructure of the fracture, polished and thermally etched (900 °C, 30 min) surfaces of the sintered materials were investigated by scanning electron microscopy (SEM) (Leica Cambridge Stereoscan 360) coupled with an energy-dispersive X-ray spectrometer (EDS). The phases were identified by a powder X-ray diffraction technique (XRD) (Rigaku, Mod. Miniflex) in the 2θ range 4–64°. Apparent density of sintered samples was measured by the Archimede's method in water.

The surfaces of the sintered samples were grinded, silver electroded on the major faces and poled under a field of 3 kV/mm at 120 °C for 40 min. An HP4194 impedance analyser was used to determine the piezoelectric constants by the IEEE (176-1987) resonance method.

3. Results and discussion

3.1. Precursor solution and powder synthesis

The efficiency of the synthesis by spray drying a solution is strongly limited by the maximum concentration of the salts in the precursor solutions. In this case, as the four salts show the maximum solubility in different conditions, the concentration of the multi-component solution is governed by the solubility of lead and zirconium nitrates in nitric acid. The maximum concentration reachable resulted 0.2 M on lead basis at pH ≅ 1. In order to control the stability of the solutions of the four starting salts the concentration of Pb^{2+}, Zr^{4+}, Ti^{4+} and Nb^{5+} solutions was checked during the first two weeks after the preparation and the results are reported in Fig. 2. The titre of the Pb^{2+} and Nb^{5+} solutions resulted stable within the first week while the Zr^{4+} and Ti^{4+} solutions were stable within the whole observed period. In Table 1 the molar ratios of elements referred to solution, as-sprayed, calcined and sintered samples are reported and compared to the nominal composition. The molar ratios of powder 2 are in agreement with the nominal stoichiometry while powder 1 shows a slight Pb excess in comparison to the expected Ti + Zr molar amount and a slight defect of Ti with respect to the nominal Ti/Zr molar ratio. The composition, controlled after every critical step of the process, resulted almost unchanged for both batches (Table 1). Both powders 1 and 2 were processed in order to evaluate the effect of a slight fluctuation of the stoichiometry on the physical and electrical properties of the final bodies.

3.2. Morphology

In a preliminary step the titanium solution was investigated to study the influence of the spray-drying conditions on the morphology of the powders. Four batches were spray

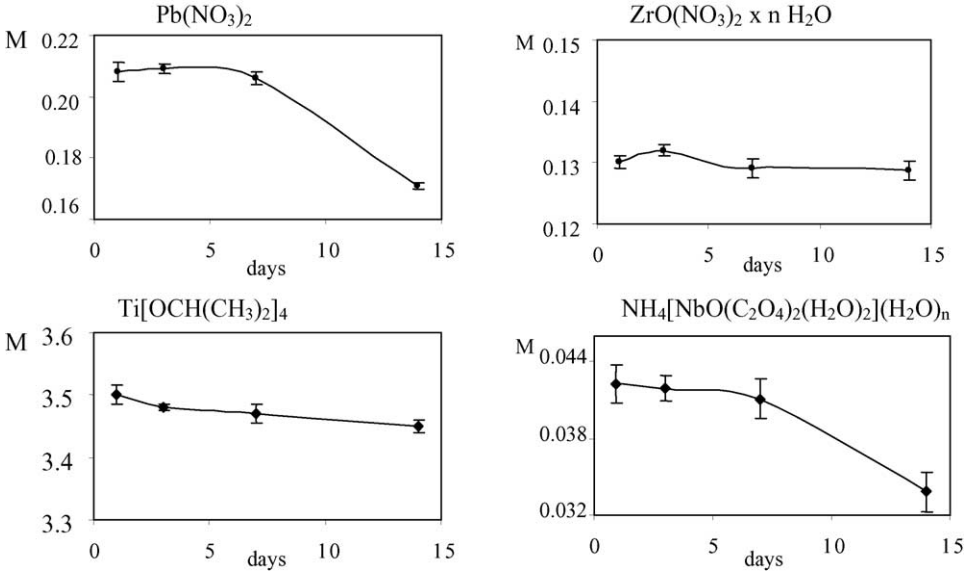

Fig. 2. Molarities of Pb^{2+}, Zr^{4+}, Ti^{4+} and Nb^{5+} solutions during the first two weeks.

Table 1
Elemental analysis at the different steps of the process

Element	Nominal	Solution 1	Solution 2	As-sprayed 2	Calcined (2B)	Sintered (2B)
Pb	1.000	1.000 ± 0.002	1.000 ± 0.002	1.000 ± 0.004	1.000 ± 0.004	1.000 ± 0.009
Zr	0.514	0.511 ± 0.009	0.520 ± 0.005	0.517 ± 0.002	0.516 ± 0.002	0.520 ± 0.005
Ti	0.480	0.457 ± 0.005	0.466 ± 0.005	0.480 ± 0.001	0.480 ± 0.004	0.487 ± 0.005
Nb	0.024	0.023 ± 0.001	0.024 ± 0.001	0.023 ± 0.001	0.024 ± 0.001	0.023 ± 0.001

The compositions are expressed in terms of molar ratio referred to lead. The absolute error reported depends on different procedures used in the preparation of the samples for ICP and on the number of analyses performed for each sample.

Table 2
Spray drier conditions for the atomisation of titanium solution

	Batch			
	1, mixed[a]	2, mixed[a]	3, co-current[a]	4, co-current[a]
Pump suction flow (ml/h)	650	650	170	170
Atomising air pressure (bar)	1.2	3.5	1.2	3.5
Air stream temperature (°C)	220	250	220	250

Air flow fixed at 56 m^3/h. Nozzle diameter: 0.5 mm.
[a] Flow configuration.

dried using different spray-drying configurations (Table 2). In particular two different configurations of the flow direction were chosen. In the mixed flow configuration the feeding solution is sprayed from the bottom of the vessel and mixed with the heating air flowing from the top. This arrangement causes growth of the liquid droplets as a consequence of the collision of partially dried particles with the ascending liquid droplets. In the co-current configuration, both the solution

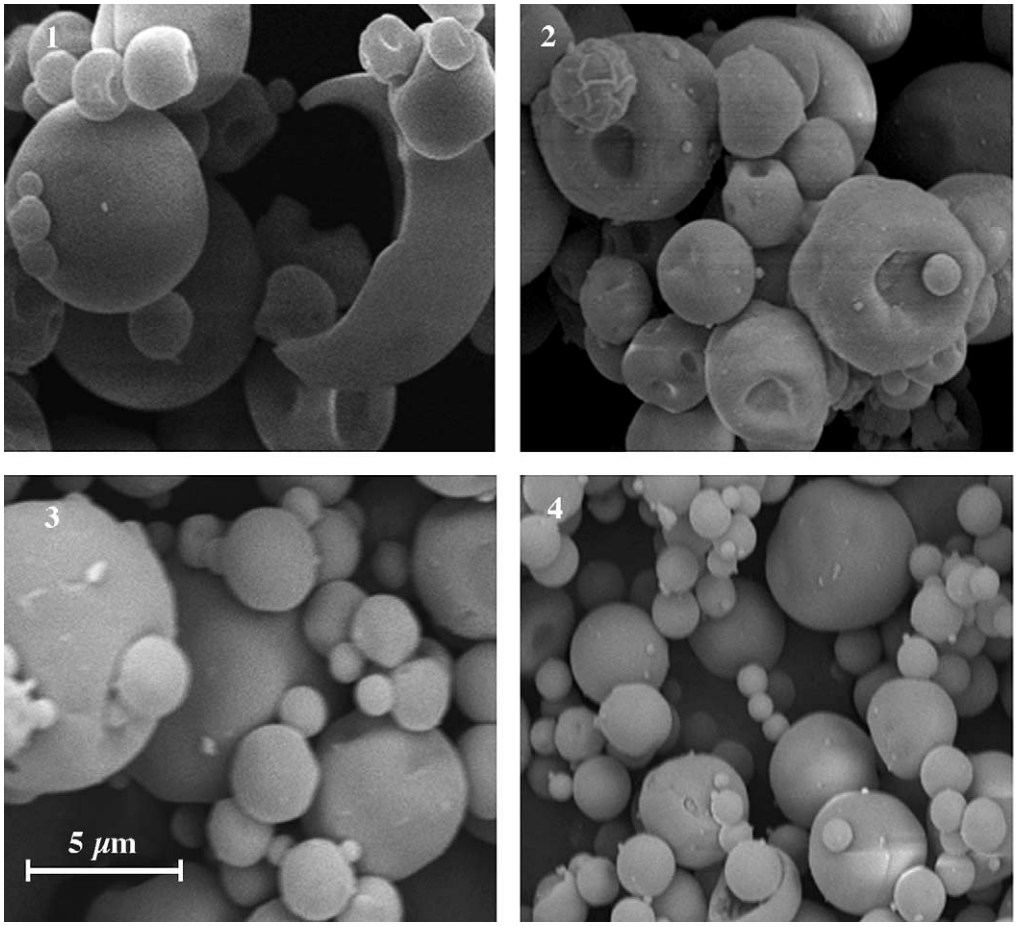

Fig. 3. Morphologies of $Ti[OCH(CH_3)_2]_4$ solution derived powders, spray-dried in different conditions. The spray drying configurations relative to batches 1–4 are reported in Table 2.

droplets and the heating air flow from the top of the chamber resulting in a lower contact time and smaller mean size of the agglomerates, even if the atomising air pressure remains the critical parameter to control the agglomerate size. The as-sprayed powders were observed by SEM and the results are shown in Fig. 3. The change of the spray-drying configurations induced a change in the morphology of the particles due to surface or volume precipitation. The frequency and mode of fracture of broken agglomerates suggested the prevalence of surface precipitation mechanism in the batches 1 and 4. The processing conditions of batch 3 induced volume precipitation that leaded to filled agglomerates with a bimodal size distribution. This powder morphology is generally required to obtain very dense material. The particles from batch 2 were filled too but with an evident collapse of a part of the surface due to internal shrinkage as a consequence, most probably, of an higher degree of porosity. The spraying conditions of the single cation solutions were found to be different from the ones used to spray the complete mixture. A general correlation between particle morphology and spray-drying conditions resulted very difficult because the characteristics of the solutions in terms of viscosity, concentration of saturation, and chemical stability are fundamental in order to influence the precipitation mechanism and consequently the particle morphology. The spray-drying conditions also influence the yield of the process. The latter is improved by an increase of agglomerate size and degree of dryness. The mixed flow configuration allows a more efficient drying and

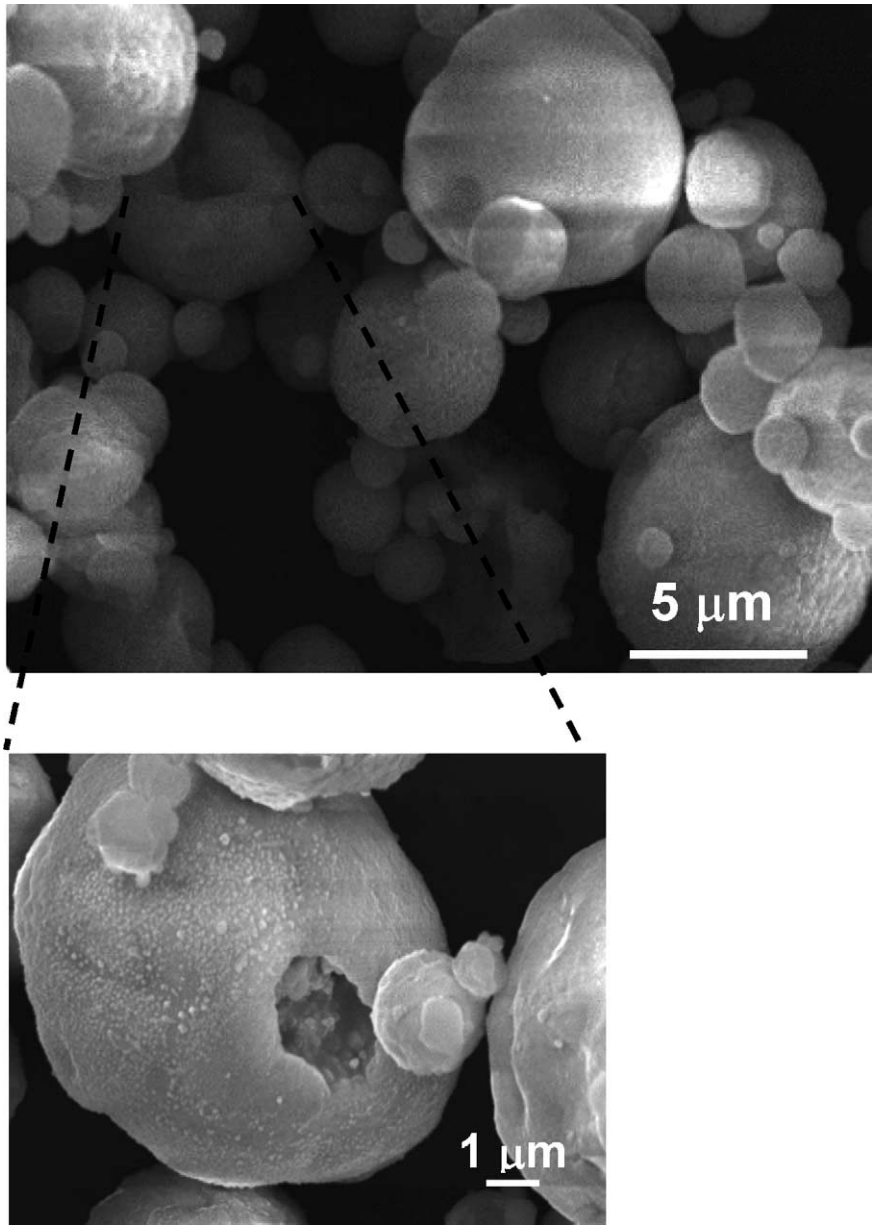

Fig. 4. Morphology of PZTN precursor solution spray dried with mixed flow at pump suction flow 286 ml/h, air flow 66 m^3/h, atomising air pressure 2.5 bar, nozzle diameter 0.5 mm, air stream temperature 220 °C.

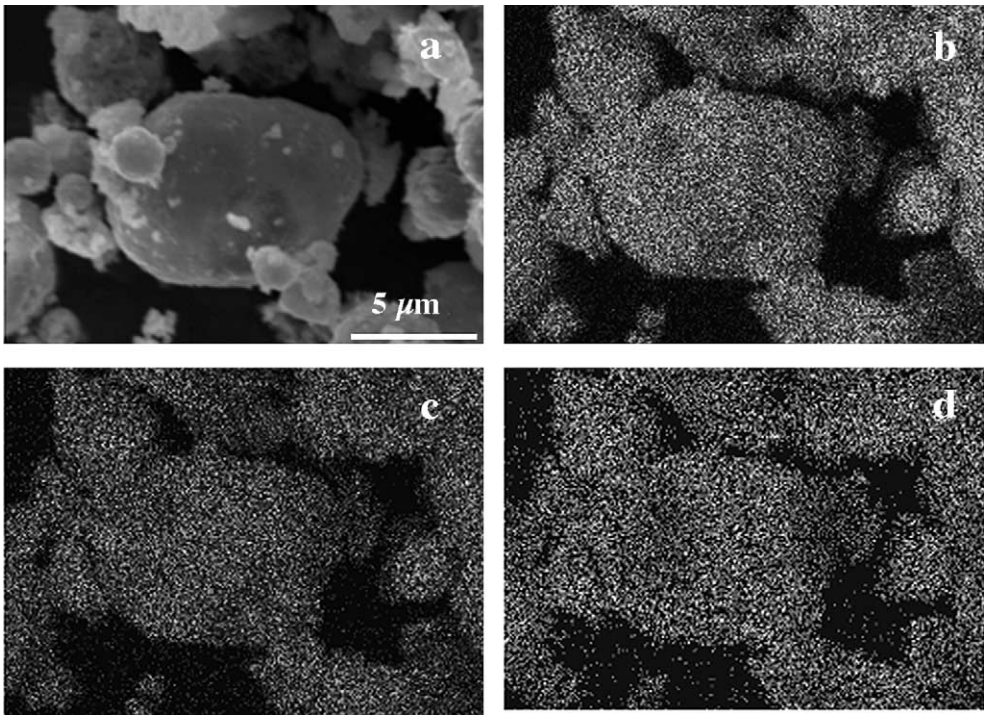

Fig. 5. Distribution of Pb^{2+} (b), Zr^{4+} (c) and Ti^{4+} (d) cations in the as-sprayed PZTN precursor powder (a).

a low atomising air pressure favours large agglomerate size. These conditions were therefore chosen as driving parameters for the spraying of the multi-component solution. The morphology of the as-sprayed powder is shown in Fig. 4. As-sprayed particles resulted porous (tapped density about 30% of theoretical density) and spherical, with diameter in the range of 0.5–15 μm. The spheres are aggregates of crystallites (mean dimension around 100 nm) uniformly distributed throughout the volume.

SEM micrograph of PZTN precursor powder together with Pb, Zr and Ti maps are shown in Fig. 5. This analysis evidences an homogeneous distribution of elements on the surface of the agglomerates. Considering the fast solvent evaporation into the chamber, any further segregation inside the particles can be excluded. This result is important in order to prevent the formation of secondary phases as a consequence of volume segregation.

3.3. Thermal analysis

DTA and TG analysis of the precursor powders of the separate cations and of the multi-component mixture are reported in Fig. 6. The analysis on powder derived from the lead solution (Fig. 6a) shows a single endothermic peak with a weight loss of more than 20% at about 500 °C. This corresponds to the decomposition of lead nitrate that is reported at 470 °C.[29] The analysis on powder derived from Ti solution (Fig. 6c) shows a single endothermic peak at 150 °C with a 50% weight loss associated to the evaporation of adsorbed water and to the decomposition of metal-organic groups. The latter takes place at lower temperature than the decomposition of inorganic salts. The analysis on powder derived from Nb and Zr solution show a multi-step decomposition. The $ZrO(NO_3)_2$ (Fig. 6b) exhibits two endothermic peaks at about 140 and 260 °C and an exothermic peak at about 470 °C that corresponds to the final decomposition of nitrate with a total weight loss of about 45%. The decomposition of the peroxo-niobium complex (Fig. 6d) starts with an endothermic peak at around 100 °C associated to the evaporation of the adsorbed water (weight loss of about 15%) and an endothermic peak at 270 °C with a total weight loss of about 65%. The TG analysis of the PZTN solid precursor (Fig. 6e) evidences a slow weight loss between 100 and 420 °C with a rapid increase passing from about 25 to 40% up to 500 °C. From the DT analysis, the endothermic peak at about 100 °C is attributed to the water evaporation and titanium isopropoxide decomposition. The endothermic peaks at about 300, 450 and 500 °C are attributed to the decomposition of nitrates. In particular the decomposition of lead nitrate into oxides takes place with a three steps mechanism as reported elsewhere[30]:

$$3Pb(NO_3)_2 \rightarrow Pb(NO_3)_2 \cdot 2PbO + 4NO_2 + O_2$$

(290–340 °C)

$$4(Pb(NO_3)_2 \cdot 2PbO) \rightarrow 2(Pb(NO_3)_2 \cdot 5PbO) + 4NO_2 + O_2$$

(400–460 °C)

$$2(Pb(NO_3)_2 \cdot 5PbO) \rightarrow 12PbO + 4NO_2 + O_2$$

(480–520 °C)

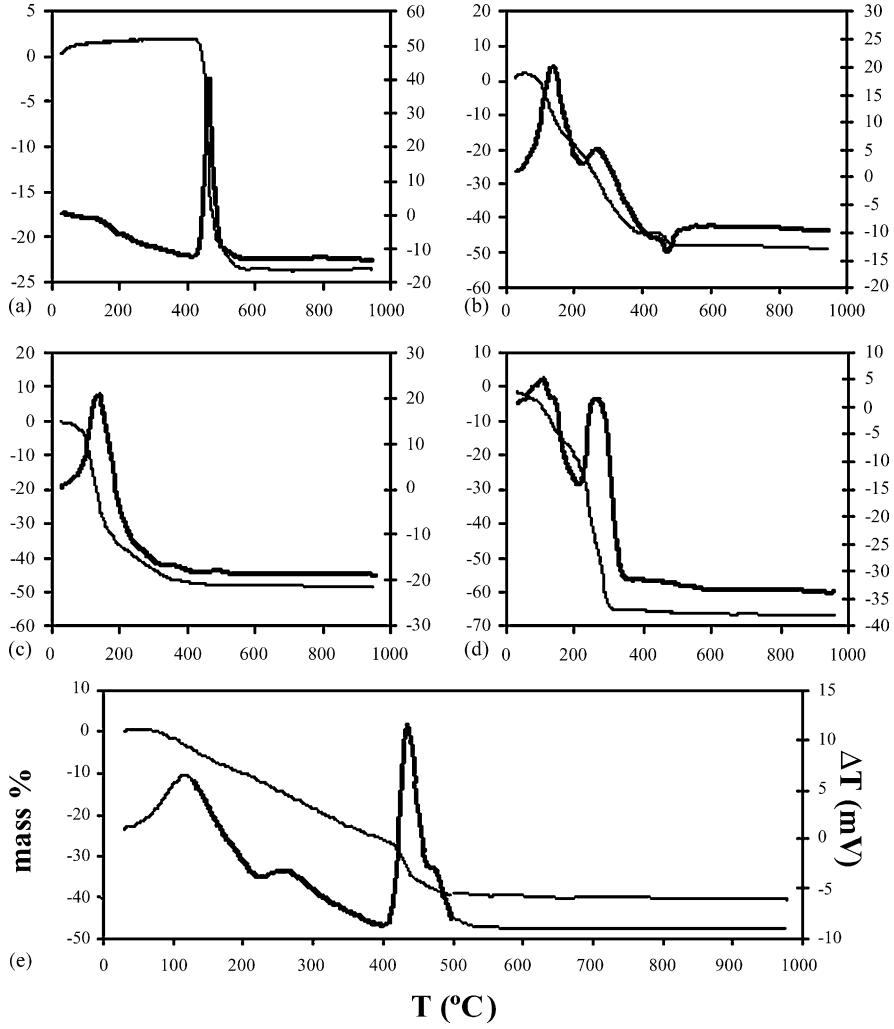

Fig. 6. Thermal analysis of $Pb(NO_3)_2$ (a), $ZrO(NO_3)_2{\cdot}nH_2O$ (b); $Ti[OCH(CH_3)_2]_4$ (c); $NH_4[NbO(C_2O_4)_2(H_2O)_2](H_2O)_n$ (d) and PZTN (e) solution derived powders.

The three steps are not detectable from the graph because the scale enlargement necessary to include the transformation at 470 °C does not allowed the appropriate reduction. The peak relative to this transformation masks the formation of the perovskite phase at 550 °C, as shown by the XRD analysis.

3.4. Calcination to the perovskitic phase

The XRD patterns of the as-calcined powders is reported in Fig. 7. At 400 °C the powder is only partially crystallised and shows traces of an intermediate $PbO_{1.44}$ phase among the amorphous phase of precursors. On the other hand at 550 °C the formation of the perovskite phase is complete. The enlarged peaks are due to the low crystallinity degree achieved at this temperature. The diffactogram at 800 °C does not change and for this reason 550 °C was chosen as temperature for the formation of pure perovskite phase of the SD powder. The MO powders are less reactive so that for the same soaking time (4 h), higher temperature (about 850 °C) is necessary to obtain the perovskite phase.

The morphology of the powders calcined at different temperature are shown in Fig. 8. The porous spheres are aggregates of crystallites (mean dimension around 100 nm) that are uniformly distributed throughout the volume as showed

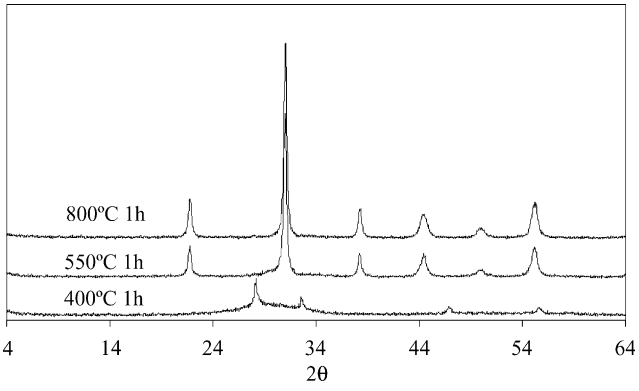

Fig. 7. XRD pattern of the PZTN solid precursor calcined at 400, 550 and 800 °C.

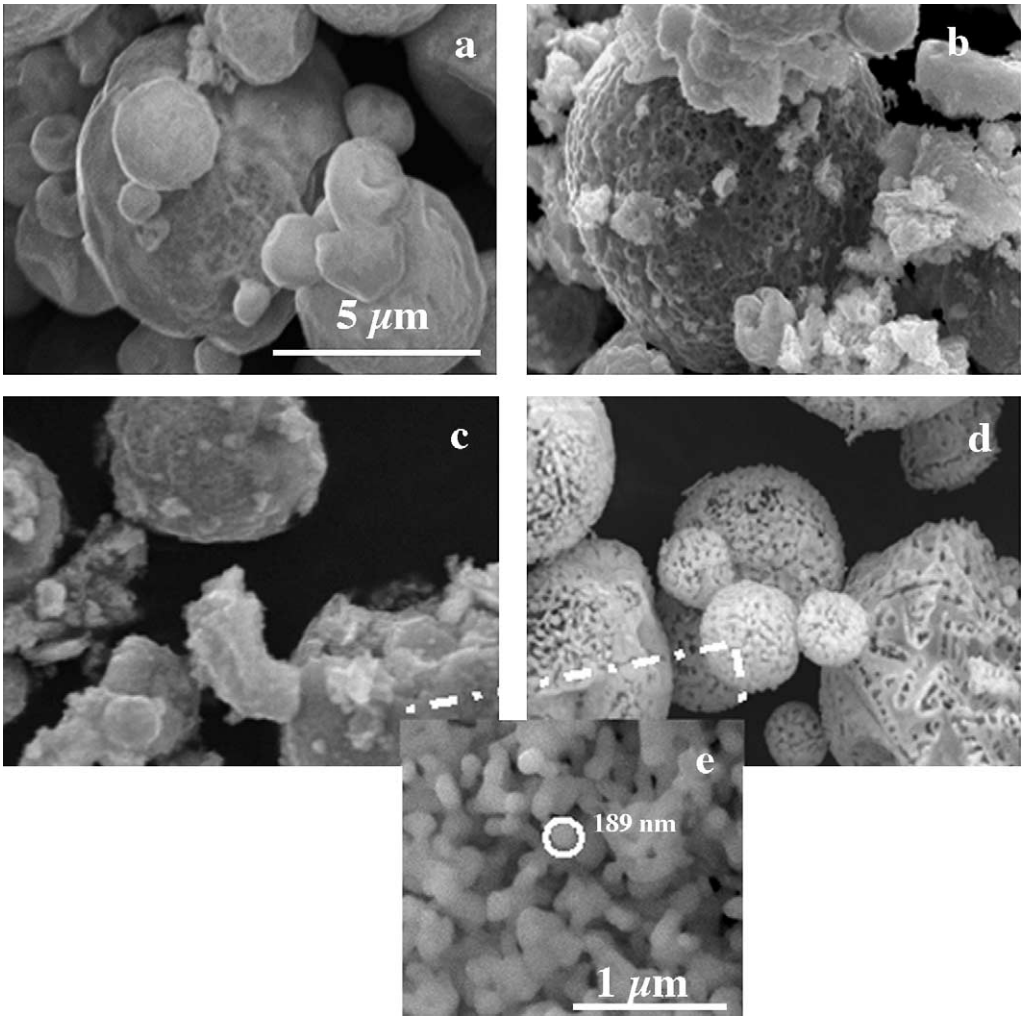

Fig. 8. SEM morphologies of powders: A, calcined at 400 °C (a); B, calcined at 550 °C (b); C, calcined at 550 °C and ball milled (c); D, calcined at 800 °C (d) with enlargement of the primary particles structure (e).

by SEM micrographs of powders B, C and of the powder calcined at 800 °C. The morphology of filled spheres indicates that the spray-drying conditions used and the characteristics of the precursors allow a volume precipitation. The aggregates of powder C result partially broken due to the ball milling treatment. Calcination at 800 °C (powder D) induces partial sintering that better evidences the typical structure of SD particles finely subdivided into sub micron sized crystallites.

3.5. Cold consolidation

The process parameters, green and sintered densities are shown in Table 3. The spray-dried powders A and B lead to lower values of green density (about 50% theoretical density) in comparison to MO powder (about 60% theoretical density). The wet ball milling treatment carried out to crush the agglomerates improves substantially the compaction behaviour, achieving for powder C almost the same green density of MO powder (about 57% theoretical density). MO powder with a narrower size distribution shows a very good cold packing that allows to reach 61% relative density already at low pressure (150 MPa).

3.6. Sintering

The sintering parameters were modified in order to find the optimal conditions for the full densification of the highly reactive spray dried powders (Table 3). The influence of the slight lead excess in the composition and the calcining temperature were also considered.

The slight lead excess is expected to promote the formation of transient liquid phase that remain as a residual intergranular phase after sintering. Although it is not detected in the bulk material, the XRD analysis of the surface of the as sintered samples evidences traces of lead oxide. The lead-rich intermediate phase is evidenced by the large PbO reach PbO/ZrO_2 inclusions grown on the polished surfaces of 1 samples (and not on samples 2) after thermal etching (900 °C for 15′) as can be noted in Fig. 9. The process of migration, vaporisa-

Table 3
Process parameters and physical properties of sintered samples

Sample	Sintering temperature (°C)	Green density		Weight loss (%)	Linear shrinkage (%)	Sintered density		Mean grain size (μm)[b]
		(g/cm[c])	(%)			(g/cm[c])	(%)[a]	
1-A-1	1000	3.75	47	5.4	20.81	7.40	92.0	0.40
1-A-2	1100	3.75	47	5.6	22.51	7.93	99.0	0.70
1-B-1	900	4.20	53	1.1	4.38	7.33	92.0	
1-B-2	1000	4.17	52	1.1	18.09	7.65	96.0	0.40
1-B-3	1100	4.16	52	1.4	18.61	7.90	99.0	0.70
2-A-1	1100	3.79	47	5.9	22.49	7.84	97.9	1.0
2-B-1	1100	4.08	51	0.3	19.18	7.83	97.8	0.8
2-B-2[c]	1100	4.07	51	0.2	19.18	7.83	97.8	1.0
2-C-1	1100	4.58	57	2.7	15.93	7.91	98.7	0.8
2-C-2[d]	1100	4.58	57	2.4	15.67	8.01	100.0	1.2
MO	1250	5.00	63	1.1	12.82	7.82	97.7	0.9

[a] Theoretical density: 8.006 g/cm^3 (JCPDS: 33-783).
[b] Determined by SEM photographs with the linear intercept technique.
[c] Post-annealing of 1100 °C (2 h).
[d] Post-hipped.

tion and re-crystallisation of a PbO-rich liquid phase towards the top air surfaces of lead-based perovskite was already noted elsewhere.[31] The presence of this PbO liquid phase gives reason of the better densification of sample 1 compared with 2.

The amorphous SD powder A results almost fully dense (sample 1-A-1 and 2-A-1, 99 and 97.9% theoretical density). This result stresses the high reactivity of powder calcined at 400 °C that forms the perovskitic phase during sintering. The direct synthesis of perovkite phase during sintering starting

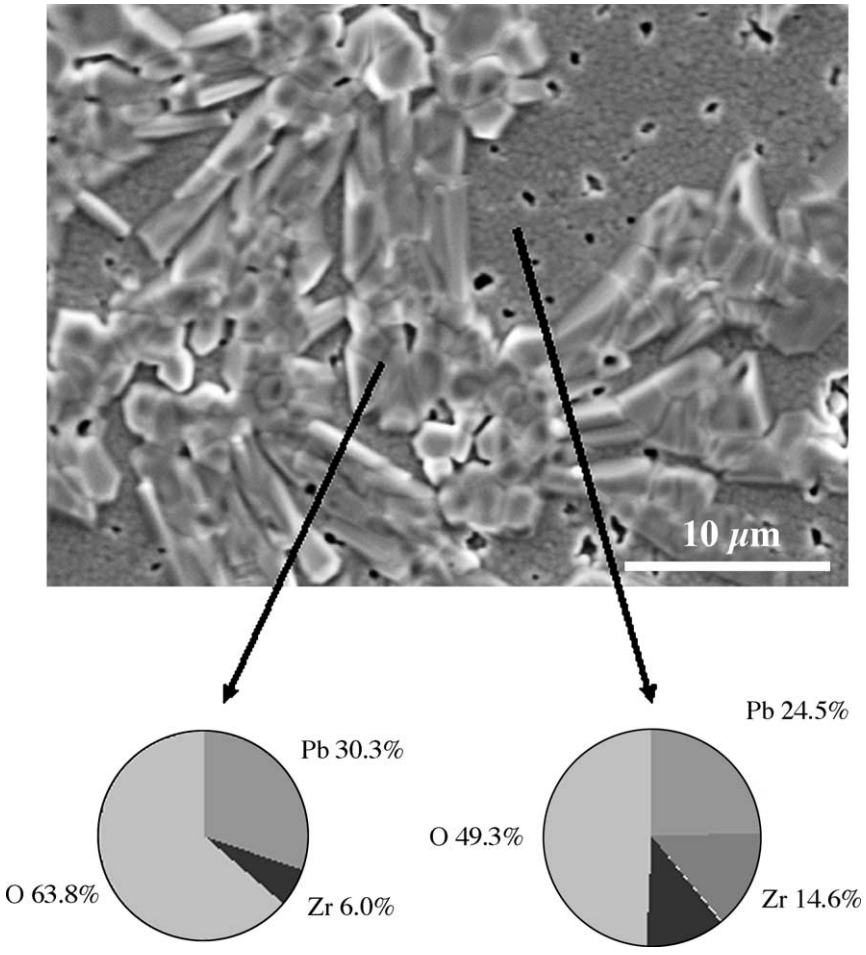

Fig. 9. SEM morphologies of sample 1-B-3 after thermal etching (900 °C for 15′).

from SD powders was detected in a previous work.[32] The SD powder B that forms the perovskitic phase at 550 °C leads to a final density of 99.0 and 97.8% upon sintering at 1100 °C for 2 h, samples 1-B-3 and 2-B-1, respectively.

The grinding treatment of SD powder C increases the sinterability of powder calcined at 550 °C. A final density of 98.7% can be achieved at 1100 °C for 1 h (sample 2-C-1). The HIP post-treatment further improves the final density to the theoretical density for sample 2-C-2.

The XRD spectra recorded on sintered samples show the coexistence of rombohedral and tetragonal perovskite phases with a rhombohedral to tetragonal phase evolution upon heating that is similar for the two processing procedures (SD and MO).

3.7. Microstructure

SEM micrographs of fracture, polished and thermally etched surfaces of the sintered bodies obtained by powders A and B are shown in Fig. 10. The calcination temperature (400 °C for sample A-1 and 550 °C for samples B-1 and B-2) and the soaking time (2 h for samples A-1 and B-1 and 4 h for sample B-2) do not affect the mean grain size (about 1.3 μm). In the sample A-1 it is evident the presence of ag-

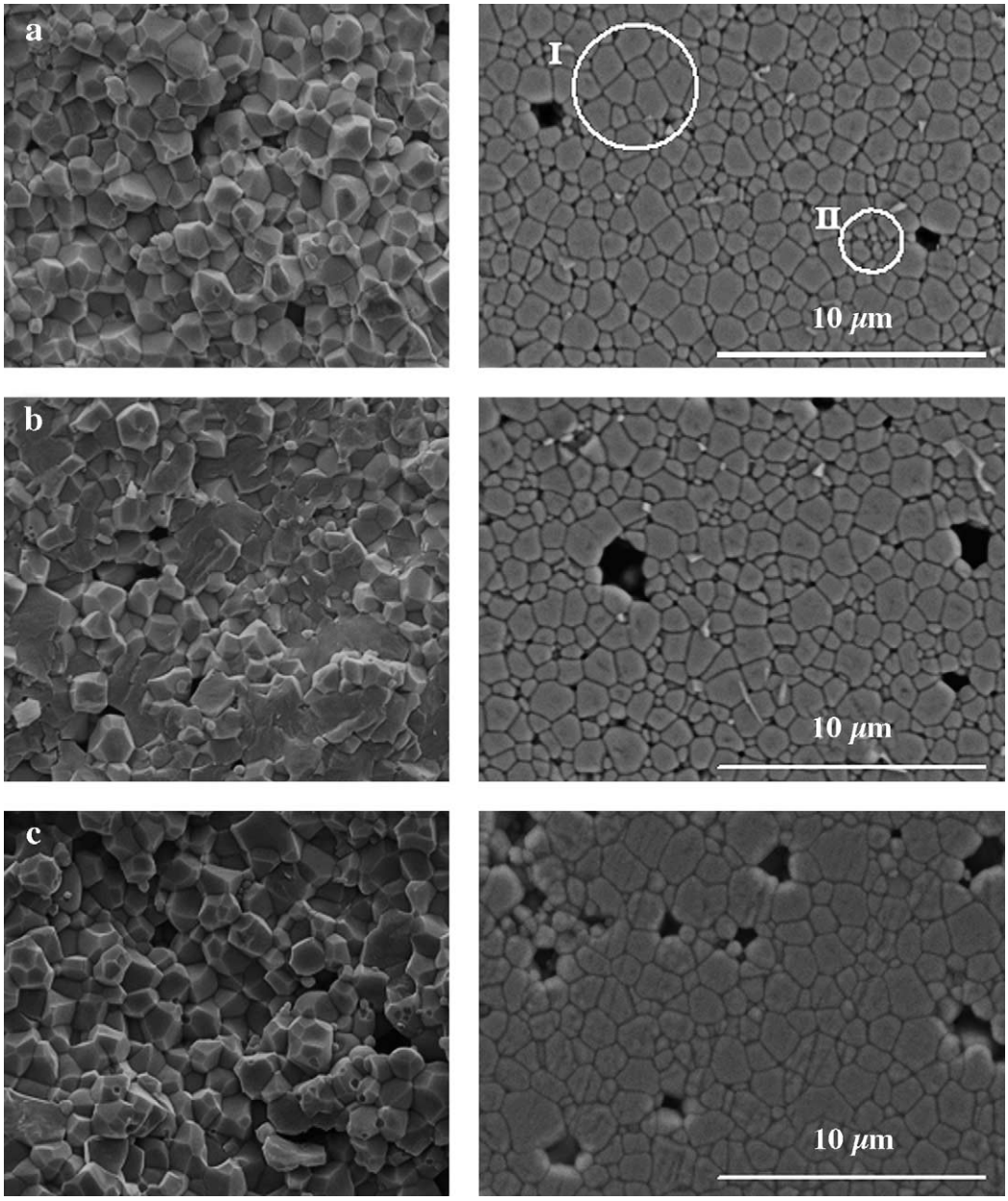

Fig. 10. SEM micrographs of fracture, polished and thermally etched surfaces of (a) 2-A-1 (400 °C/1100 °C 2 h); (b) 2-B-1 (550 °C/1100 °C 2 h; (c) 2-B-2 (550 °C/1100 °C 4 h).

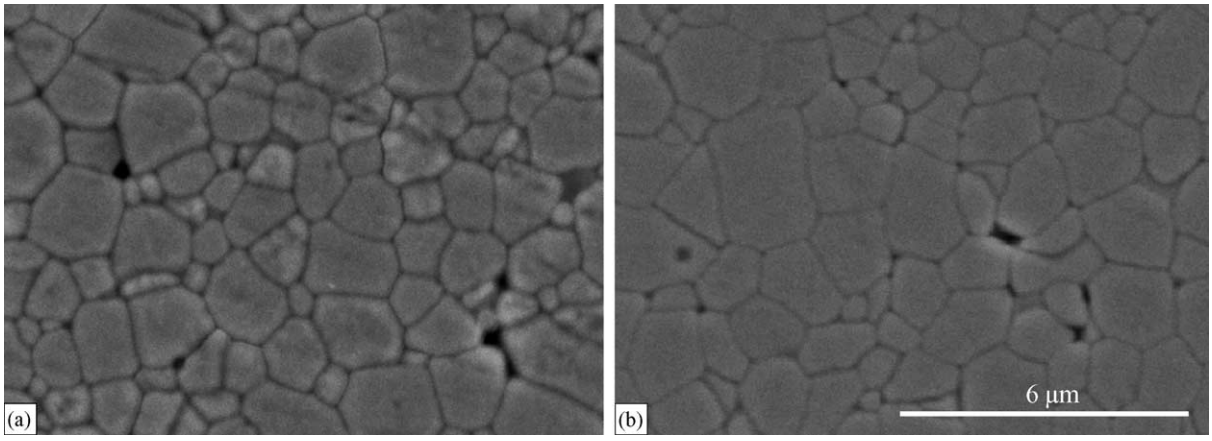

Fig. 11. SEM micrographs of thermally etched surfaces of (a) 2-C-1 (550 °C/1100 °C 2 h) and (b) 2-C-2 (550 °C/1100 °C 2 h, HIP: 1100 °C 2 h, 30 MPa).

Table 4
Electric and piezoelectric properties

Sample	ρ (%)	ε_{33}^{T}	k_p	k_{31}	d_{31} 10^{-12} m/V	d_{33} 10^{-12} m/V
MO	97.7	1551	0.670	−0.380	−184	355
2-A-1	97.9	1401	0.315	−0.166	−63	180
2-B-1	97.8	1644	0.544	−0.287	−127	335
2-B-2	97.8	1569	0.454	−0.238	−107	280
2-C1	98.7	1727	0.620	−0.336	−165	349
2-C-2	100.0	1546	0.617	−0.335	−152	328

	s_{11}^{E} (10^{-12}m^2/N)	Q_m	σ^E	v_1^E [m/s]	Z_a (10^6Kg/(m^{2}s))
MO	16.70	84.6	0.350	2767	21.6
2-A-1	44.68	72.2	0.443	3306	25.9
2-B-1	13.47	67.4	0.444	3079	24.1
2-B-2	14.62	68.2	0.447	2955	23.2
2-C1	15.72	88.7	0.413	2837	22.4
2-C2	15.10	69.8	0.410	2874	23.1

gregates with mean size 2 μm (I) and lower than 500 nm (II). The powder calcined at 400 °C results more reactive in comparison with the powder calcined at 550 °C and the regions with bigger grain size are due to the grain growth process that follows the sintering (Fig. 10a). The microstructure of sample B1 shows a more homogenous distribution of big and small grains that induces transgranular fracture type (Fig. 10b). The microstructure of sample B-2 evidences a further coalescence of small grains that leaves behind some macroporous responsible for a intergranular fracture type (Fig. 10c). In Fig. 11 the thermally etched surfaces of samples sintered from crushed powder are shown. During post-hipping treatment the average size of the grains increases (from 1 to 1.2 μm) but the gas pressure leads to reach a final density of 100%. The MO samples show microstructures very similar to those derived by spray drying process.

3.8. Piezoelectric properties

The electric and piezoelectric constants are reported in Table 4. SD materials show comparable and sometimes higher values of the main piezoelectric constants in comparison with MO materials. The better results in terms of dielectrical properties and efficiency of electromechanical coupling are obtained for samples derived by powder C. The grinding treatment that increases the cold consolidation behaviour and, as a consequence, the microstructural characteristics, improves also the piezoelectric performances. The fully densified sample by post-hipping does not show improved electrical properties. The optimisation of the post-hipping treatment and particularly the possibility of making the process under oxygen atmosphere is still in progress in order to increase benefit of hot isostatic pressing treatment.

4. Conclusions

Nb-doped $Pb(Zr,Ti)O_3$ powders were synthesised by spray drying the solution of the precursors followed by calcination. The formation of pure perovskitic phase at 550 °C confirmed the potentiality of spray drying as a simple synthesis process to produce chemically homogeneous and very reactive powders. Spherical agglomerates are obtained with a density gradient from the shell towards the inner part, the pri-

mary particles size being in the nanometric range. The cold compaction behaviour and the green density of the samples were optimised introducing a grinding step after calcination. The samples prepared by spray drying reach full density at lower temperatures with respect to the ones conventionally prepared. The final density and microstructures are improved by hot isostatic pressing treatment. The piezoelectric properties obtained are comparable or better than those from conventional mixed oxide route.

Acknowledgements

We gratefully acknowledge Dr Elena Landi for thermal analyses and Silvano Tarlazzi for XRD analyses.

References

1. Choy, J. H., Han, Y.-S. and Kim, J. T., Hydroxide coprecipitation route to the piezoelectric oxide. *J. Mater. Chem.*, 1995, **5**(1), 65–69.
2. Lemoine, L., Leriche, A. and Thierry, B., PZT powder synthesis through coprecipitation route. In *Third Euroceramics, Vol I*, ed. P. Duran and J. F. Fernandez. Faenza Editrice Iberica Castellon de la Plana, 1993, pp. 317–322.
3. Villegas, M., Moure, C., Jurado, J. R. and Duran, P., Influence of the calcining temperature on the sintering and properties of PZT ceramics. *J. Mater. Sci.*, 1993, **28**, 3482–3488.
4. Akbas, M. A. and Lee, W. E., Characterization and densification of PLZT powder coprecipitated from chloride-nitrate solutions. *Br. Ceram. Trans.*, 1996, **95**, 49–52.
5. Leite E. R., Longo, E., Cavaco, M. C. S., Carvalho, L. C., Avena, J. and Varela, J. A., Synthesis of (Nb Sr) doped PZT by partial oxalate method. In *Third Euroceramics, Vol I*, ed. P. Duran and J. F. Fernandez. Faenza Editrice Iberica Castellon de la Plana, 1993, pp. 309–315.
6. Ohba, Y., Rikitoku, T., Tsurumi, T. and Daimon, M., Precipitation of lead zirconia titanate powders under hydrothermal conditions. *J. Ceram. Soc. Jpn. Int.*, 1990, **104**, 8–12.
7. Lencka, M., Anderko, A. and Riman, R. E., Hydrothermal precipitation of lead zirconate titanate solid solutions: thermodynamic modelling and experimental synthesis. *J. Am. Ceram. Soc.*, 1995, **78**(10), 2609–2618.
8. Lemoine, L., Leriche, A., Tronc, P. and Thierry, B., Optimisation of synthesis parameters of PZT powder through hydrothermal routes. In *Third Euroceramics, Vol I*, ed. P. Duran and J. F. Fernandez. Faenza Editrice Iberica Castellon de la Plana, 1993, pp. 350–355.
9. Kholkin, A. L., Yarmarkin, W. K., Wu, A., Avdeev, M., Vilarinho, P. M. and Baptista, J. L., PZT-based piezoelectric composites via a modified sol–gel route. *J. Eur. Ceram. Soc.*, 2001, **21**, 1535–1538.
10. Tartaj, J., Moure, C., Lascano, L. and Duran, P., Sintering of dense ceramics bodies of pure lead titanate obtained by seeding-assisted chemical sol–gel. *Mater. Res. Bull.*, 2001, **36**, 2301–2310.
11. Surowiak, Z., Kupriyanov, M. F. and Czekaj, D., Properties of nanocrystalline ferroelectric PZT ceramics. *J. Eur. Ceram. Soc.*, 2001, **21**, 1377–1381.
12. Liu, C., Zou, B., Rondinone, A. J. and Zhang, Z. J., Sol–gel synthesis of free-standing ferroelectric lead zirconate titanate nanoparticles. *J. Am. Chem. Soc.*, 2001, **123**, 4344–4345.
13. Kim, B.-H., Ueda, K., Sakurai, O. and Mizutani, N., Synthesis of Pb $(Mg_{1/3}Nb_{2/3})O_3$ powder by the spray pyrolysis with ultrasonic atomizer. *J. Ceram. Soc. Jpn. Int.*, 1992, **100**, 258–261.
14. Takigawa, K., Nonaka, K., Okada, K. and Otsuka, N., Preparation of PLZT fine powders by the spray pyrolysis method. *Br. Ceram. Trans. J.*, 1990, **89**, 82–86.
15. Kim, H.-B., Lee, J.-H. and Park, S. J., Preparation of spherical $Pb(Zr,Ti)O_3$ by ultrasonic spray pyrolysis. *J. Mater. Sci.: Mater. Electron.*, 1995, **6**, 84–89.
16. Nimmo, W., Ali, N. J., Brydson, R. M., Calvert, C., Hampartsoumian, E., Hind, D. *et al.*, Formation of lead zirconate titanate powders by spray pyrolysis. *J. Am. Ceram. Soc.*, 2003, **86**(9), 1474–1480.
17. Thomson, J., Chemical preparation of PLZT powders from aqueous nitrate solutions. *Am. Ceram. Soc. Bull.*, 1974, **53**(5), 421–424/433.
18. Weddigen, A., Hennige, V. D., Gunther, E. and Ritzhaupt-Kleissl, H.-J., Production of piezoceramic powders by the thermal two-stage process. *J. Mater. Sci.*, 1999, **34**, 3461–3465.
19. Kakegawa, K., Arai, K., Sasaki, Y. and Tomizawa, T., Homogeneity and properties of lead zirconate titanate prepared by a combination of thermal spray decomposition method with solid-phase reaction. *J. Am. Ceram. Soc.*, 1988, **71**(1), C-49–C-52.
20. Dayal, R., Prasad, C. D. and Lal, R., Calcination characteristics of spray-dried PZT and related powders. *Mater. Res. Bull.*, 1990, **25**, 1339–1346.
21. Johnson Jr., D. W., Innovations in ceramic powder preparation. In *Ceramic Powder Science*, ed. G. L. Messing, K. S. Mazdiyasni, J. W. McCauley and R. A. Haber. American Ceramic Society, Westerville, OH, 1987, pp. 3–19.
22. Sanson, A., Galassi, C., Costa, A. L. and Russo, U., Synthesis of $0.94(Bi_{1/2}Na_{1/2})TiO_3$-$0.06BaTiO_3$ by spray-drying. In *Proceedings of Ferroelectrics UK*, 2001, pp. 119–126.
23. Messing, G. L., Zhang, S.-C. and Jayanthi, G. V., Ceramic powder synthesis by spray pyrolysis. *J. Am. Ceram. Soc.*, 1993, **76**(11), 2707–2726.
24. Sproson, D. W. and Messing, G. L., Ceramic powder synthesis by thermal reaction of atomized solutions. In *Ceramic Powder Science*, ed. G. L. Messing, K. S. Mazdiyasni, J. W. McCauley and R. A. Haber. American Ceramic Society, Westerville, OH, 1987, pp. 99–107.
25. Paik, D. S. and Komarneni, S., Composites of $0.9Pb(Mg_{1/3}Nb_{2/3})O_3$-$0.1PbTiO_3$ prepared by a sol–gel method: effect of atmosphere powders. *J. Mater. Sci.*, 1999, **34**, 2313–2317.
26. Charlot, G., *Analisi chimica qualitativa; equilibri in soluzione* (*6th ed.*) Piccin Editore Padova, 1997.
27. Galassi, C., Roncari, E., Capiani, C. and Costa, A. L. Influence of processing parameters on the properties of PZT materials. In *Piezoelectric Materials: Advances in Science, Technology and Applications*, NATO ASI Series ed. G. Galassi, M. Dinescu, M. Sayer and K. Uchino. Kluwer Academics, Dordrecht, 2000, pp. 75–86.
28. Larre, M. T., Gómez-Pinilla, I. and Farinas, J. C., Microwave-assisted acid dissolution of sintered advanced ceramics for inductively coupled plasma atomic emission Spectrometry. *J. Anal. At. Spectrom.*, 1997, **12**, 1323–1332.
29. *CRC Handbook of Chemistry and Physics*, 1996.
30. Stern, K. H., High temperature properties and decomposition of inorganic salts. Part 3: nitrates and nitrites. *J. Phys. Chem. Ref. Data*, 1972, **1**, 747–772.
31. Costa, A. L., Galassi, C., Fabbri, G., Roncari, E. and Capiani, C., Pyrochlore phase and microstructure development in lead magnesium niobate materials. *J. Eur. Ceram. Soc.*, 2001, **21**, 1165–1170.
32. Costa, A. L., Galassi, C. and Roncari, E., Direct synthesis of PMN samples by spray-drying. *J. Eur. Ceram. Soc.*, 2002, **22**, 2093–2100.